Supporting Information

for

New insights into the photocatalytic mechanism of tire wear particles: Synergistic effects of surface functional components and self-releasing active factors

Kun Li (✉)[1, 2], Weiyi Li[1, 2], Zhangle Chen[1, 2], Zidong Ye[1, 2]

1 School of Environmental Science and Engineering, Nanjing University of Information Science and Technology, Nanjing 210044, China

2 Jiangsu Key Laboratory of Atmospheric Environment Monitoring and Pollution Control, Jiangsu Collaborative Innovation Center of Atmospheric Environment and Equipment Technology, Nanjing 210044, China

This Supporting Information includes a total of 34 Pages (including this page) with 10 Text, 9 Tables, 8 Figures and References.

✉ Corresponding author
E-mail: 003405@nuist.edu.cn

Text S1. Preparation of B-TWPs

The study utilized the HSU500 indoor road simulator (TMS International) following our validated protocol (Science of the Total Environment 942 (2024) 173716). The system features a programmable drum coated with asphalt-concrete (10 mm thickness, friction coefficient $\mu=0.8\pm0.05$) to mimic urban road texture. Tyres (235/45R17 Michelin PS3) were subjected to standardized load (650 kg) and inflation pressure (240 kPa). A servo motor drove the drum at 60 km/h to induce 30-minute "burnout" conditions for B-TWPs generation. Ambient temperature (25±2°C) and humidity (50±5% RH) were logged via a PLC system (1 Hz sampling). Post-collection, particles were sieved through 100-mesh stainless steel filters (150 μm, ASTM E11), transferred to pre-weighed amber glass vials (Schott Duran®), purged with nitrogen, and stored at -20°C in darkness.

Text S2. Preparation of aged TWPs

A 1 g sample of B-TWPs was immersed in 1 L of pure water and subjected to accelerated photochemical aging under a cumulative photon dose of 4.74 mol/m². The experiment was conducted in a photochemical reactor equipped with multiple 500 W xenon lamps, under continuous magnetic stirring at 300 r/min.

To clarify the UV source spectrum and irradiance uniformity, the emission spectrum of the lamps was characterized, covering a wavelength range from 280 nm to 800 nm. The spectral photon flux distribution, crucial for evaluating photochemical reactivity, is provided in Fig. S1. The average optical irradiance on the sample surface was maintained at 4.6 mW/cm², with measured spatial uniformity within ±5% across the entire exposure area, ensuring consistent testing conditions for all replicates (Li et al., 2024). The aging acceleration factor is justified with reference to ASTM G154. The selected irradiance level is comparable to the natural sunlight energy of 4.36 mW/cm². According to the reciprocity principle (Schwarzschild's law) outlined in ASTM G154-16, the photodegradation rate of many materials is linearly proportional to the incident radiant exposure. Therefore, the acceleration factor for this test can be rationally estimated by the ratio of the artificial source irradiance to that of average natural sunlight (Cambier and Frankel, 2014).

Additionally, ultrapure water was added periodically to the vessel to compensate for any evaporation that occurred during UV irradiation. After 15 days, the solid particles and the leachate were collected by filtration through a 0.45 μm aqueous fiber

membrane. The Aged-TWPs (AB-TWPs) were then dried at 25 °C, while the filtrate was stored in a brown reagent bottle.

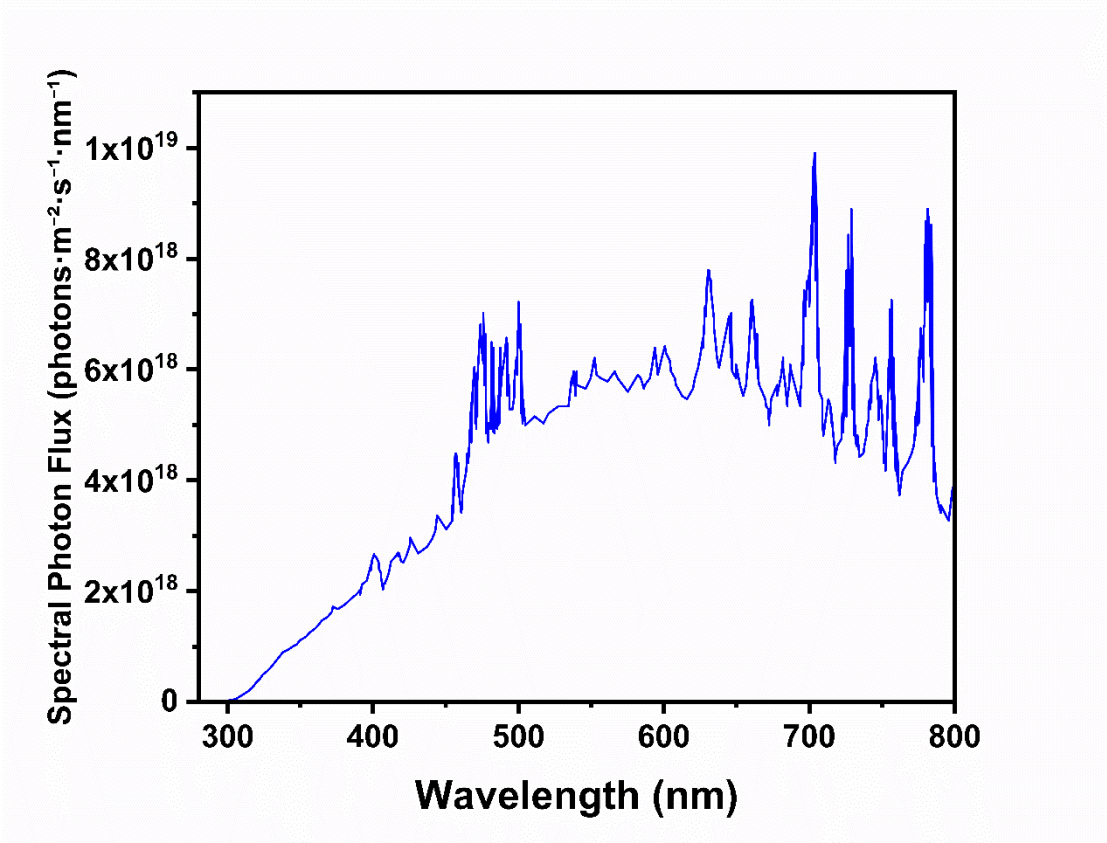

Fig. S1 Spectral Photon Flux Distribution of the Employed UV Source.

Text S3. $SUVA_{254}$ Measurement and Calculation

The aromaticity of dissolved organic matter (DOM) was assessed by measuring its specific ultraviolet absorbance at 254 nm ($SUVA_{254}$), following the established method (Abd Manan et al., 2020). Briefly, the ultraviolet absorbance at 254 nm (UV_{254}) was measured using a UV-Vis spectrophotometer with a 1 cm pathlength quartz cell, with ultrapure water serving as the blank. The dissolved organic carbon (DOC) concentration was determined by a total organic carbon (TOC) analyzer. It is important to note that since all water samples were filtered through a 0.45 μm membrane prior to analysis, the measured TOC concentration is considered equivalent to the DOC concentration for $SUVA_{254}$ calculation purposes. The $SUVA_{254}$ value (in L/mg C/m) was then calculated using the following formula:

$$SUVA_{254}\ (L\ mg\ C^{-1}m^{-1}) = UVA_{254}\ /\ TOC \times 100 \qquad Eq.S1$$

Text S4. Characteristics of TWPs

The morphology and surface physical structure of the tire wear particles (TWPs) were examined using a Scanning Electron Microscope (ZEISS Sigma 360, Germany). The samples were uniformly sprinkled onto conductive adhesive and subjected to gold sputtering under vacuum to enhance surface conductivity. Secondary electron images were acquired at acceleration voltages of 5–15 kV under high vacuum conditions to observe surface topography and micro-scale cracks (Wang et al., 2023; Wu et al., 2023). The elemental composition and distribution on the TWPs surfaces were qualitatively and semi-quantitatively analyzed using an Energy Dispersive X-ray Spectroscopy (EDS) detector coupled with the SEM. Elemental mapping and point-scan analyses were performed to determine the spatial distribution of key elements such as C, O, Zn, and Fe (Pu et al., 2025).

The surface functional groups, particularly oxygen-containing moieties, were systematically characterized using Fourier Transform Infrared (FTIR) spectroscopy (Thermo Fisher Scientific Nicolet iS20, USA). Samples were mixed with spectroscopic-grade KBr and pressed into pellets. Spectra were collected in the range of 400–4000 cm^{-1} with a resolution of 4 cm^{-1} over 32 scans per sample (Li et al., 2025).

X-ray photoelectron spectroscopy (XPS) was performed on a Thermo Scientific K-Alpha spectrometer (USA), wherein the surface composition was assessed via a wide scan and high-resolution scans of C 1s and O 1s, with all binding energies

calibrated against the C 1s peak at 284.8 eV, and the chemical states (C-C/C-H, C-O, C=O, O-C=O) were quantified by spectral deconvolution using Avantage software (Wang et al., 2023; Zhang et al., 2024). X-ray diffraction (XRD) analysis was performed on a Rigaku Ultima IV diffractometer (Japan) to determine the crystal structure and phase composition of the TWPs. The analysis utilized Cu Kα radiation under conditions of 40 kV and 40 mA, with diffraction data acquired across the 2θ range of 5–80° using a step size of 0.02° and a scanning speed of $5°\cdot min^{-1}$ (Xie et al., 2026).

Text S5. Degradation experiments

This study established two sets of experiments at different tetracycline (TC) concentrations to evaluate its degradation behavior: one involved a higher concentration referencing existing methods (20 mg TWPs in 50 mL of 50 mg/L TC), and the other involved a lower concentration more relevant to actual environmental conditions (100 μg/L TWPs and 10 mg/L TC). All experiments included blank controls and dark adsorption controls (Fan et al., 2021). A 50 mg/L TC stock solution was prepared using ultrapure water. In the reaction system, the corresponding mass of TWPs particles was mixed with 50 mL of a specific TC concentration and placed in a constant-temperature shaker at 25°C and 200 r/min. For the photodegradation experiment, the mixture was continuously stirred under simulated natural light at room temperature. Independent adsorption experiments were specifically designed and implemented to accurately calculate the actual amount of pollutants degraded by TWPs and to exclude the influence of the adsorption effect (Lei et al., 2024). Samples were collected at time intervals of 0, 1, 3, 12, 24, and 48 hours and immediately filtered through a 0.22 μm membrane to terminate the reaction. The residual TC concentration was quantified using both a UV-visible spectrophotometer and high-performance liquid chromatography (HPLC), and the degradation rate was calculated using the differential subtraction method (Xie et al., 2025). Additionally, the filtrate after 48 hours of reaction was collected, and TC degradation products were identified using liquid chromatography-mass spectrometry. The structural identifications were

assigned with confidence level 2b (probable structure) according to the Schymanski et al. framework, based on high-resolution mass spectrometry data and rational interpretation of MS/MS fragmentation patterns (Schymanski et al., 2014).

The filtrate after 48 h of reaction was taken and analyzed for TC degradation products. Chromatographic separation was carried out on a C18 column with solution A: aqueous phase (0.1% formic acid) and solution B: organic phase (100% methanol), eluting with a gradient of 5% to 95% acetonitrile for 10 min at a flow rate of 0.5 mL/min. The following linear gradient was used: 0 min 1% B, 4 min 10% B, 11.50 min 20% B, 13 min 30% B, 15 min 45% B, 18 min 50% B, 23 min 1% B, 28 min 1% B. The injection volume was 5 uL and the column oven temperature was set at 25 °C. The detection wavelength was set at 270 nm. The detection wavelength was set to 270 nm (Zhang et al., 2025).

Text S6. The Measurement of CV and EDC

Cyclic voltammetry (CV) was employed to measure the current density generated by TWPs in different reaction systems. During the CV scanning process, the working electrode potential was set between -1.6 V and 2.0 V, with a scan rate of 10 mV/s.

To analyze the photoelectrochemical properties of the samples, TWPs suspension was prepared in pure water, dropped onto ITO glass, and dried at 25℃. The i-t curve was recorded in a 0.1 mol/L phosphate buffer solution (pH 7) using a three-electrode system. In this setup, the ITO-coated TWPs served as the working electrode, a platinum plate acted as the counter electrode, and a saturated calomel electrode (SCE) was used as the reference electrode. A xenon lamp, simulating natural light conditions, was used as the light source. Under light illumination, the photocurrent density was measured to assess the impact of light exposure on the photoelectrochemical properties of the TWPs.

In order to exclude interference from oxygen in the air, the test must be performed in an anaerobic environment. The electrolyte consisted of 0.1 mol/L phosphate and 0.1 mol/L potassium chloride, buffered to pH 7. During timing and temperature measurement, 100 mL of electrolyte was added to the electrochemical cell and 200 μL of 0.01 mol/L ABTS was added to the electrochemical cell to obtain peak current. After the current stabilized, about 600 μL of model composite suspension (4 g/L) was injected and the EDC curve was measured (Zhang et al.,

2024).

EDC is calculated using the equation:

$$EDC = \times \int I_{ox} dt \,/(F \times m_{TWPs}) \qquad Eq.S2$$

where EDC is the number of electrons transferred in moles, I_{ox} is the response current, t is the time, F is the Faraday constant (96485 sA/mol$_e^-$), and m_{TWPs} is the TWPs mass of each injection reaction system.

Text S7. Measurement of ROS in degradation solution

Based on our investigation of the photodegradation process of TWPs, we observed maximum degradation efficiency after 48 hours of light exposure. This optimal time point was therefore selected for detailed mechanistic investigation of ROS involvement, consistent with established methodologies (Ding et al., 2022). Electron paramagnetic resonance spectroscopy (EPR, Bruker EMXplus-6/1, Germany) was employed as the primary analytical technique for ROS detection under standardized conditions: microwave frequency 9.85 GHz, power setting 2.02 mW, modulation frequency 100 kHz, and modulation amplitude 1.0 G. Quantitative analysis was performed using TEMPO as calibration standard with detection limits of 1.2×10^{10} spins/mm³ for •OH and 8.5×10^{9} spins/mm³ for $O_2^{\bullet-}$. Characteristic g-values were determined as $g\perp = 2.0068$, $g\parallel = 2.0315$ for EPFRs, $g = 2.0057$ for •OH, and $g = 2.0092$ for $O_2^{\bullet-}$. Spin trapping agents DMPO (for •OH and $O_2^{\bullet-}$) and TEMP (for $^1O_2$) were utilized following established protocols with appropriate controls confirming trapping specificity (Chokejaroenrat et al., 2024). The measured radical concentrations (•OH: 8.97×10^{10} spins/mm³; $O_2^{\bullet-}$: 6.94×10^{11} spins/mm³) significantly exceeded method detection limits, validating analytical sensitivity. The absence of $^1O_2$ signals suggests this species is not a primary ROS in our TWPs system, where electron-transfer pathways favoring radical formation appear dominant.

Text S8. Methodology for weighting analysis

In order to quantify the contribution of oxygen-containing functional groups and self-releasing active factors to the degradation process of the samples, a method based on the absolute value of the rate of change of the variables was used to assign weights. This method not only visualizes the importance of each variable, but also ensures the comparability of data with different magnitudes through normalization.

For each variable X_i, its rate of change (absolute value) is defined as:

$$R_i = \left| X_{i,2} - \frac{X_{i,1}}{X_{i,1}} \right| \times 100\% \qquad Eq.S3$$

where:

$X_{i,1}$: the value of the i-th variable in the initial state (B-TWPs);

$X_{i,2}$: the value of the i-th variable in the final state (AB-TWPs);

R_i: rate of change of the second variable (absolute value).

The sum of the absolute values of the rates of change of all variables is defined as:

$$S = \sum_{i=1}^{n} R_i \qquad Eq.S4$$

where:

n: total number of variables (n=2 in this study, i.e., oxygen-containing functional groups and self-releasing active factors);

S: sum of absolute values of the total rate of change.

The weight of each variable is calculated by the following formula:

$$W_i = R_i/S \times 100\% \qquad Eq.S5$$

where:

Wi: the weight of the i-th variable;

Ri: the absolute value of the rate of change of the i-th variable;

S: the sum of the absolute values of the total rate of change.

The formula normalizes the rate of change of each variable to a proportional value (percentage), thus reflecting its relative contribution to the total change.

Text S9. Formulas for calculating the carbonyl index (CI) and hydroxyl index (HI)

The calculation methods for the carbonyl index and hydroxyl index refer to previous studies (Song et al., 2017).

$$CI = A_{C=O}/A_{CH_2} \qquad Eq.S6$$

$$HI = A_{OH}/A_{CH_2} \qquad Eq.S7$$

Where:

$A_{C=O}$: Peak area of the characteristic carbonyl peak;

A_{OH}: Peak area of the hydroxyl characteristic peak;

A_{CH_2}: Peak area of the characteristic CH_2 methylene carbonyl peak.

Text S10. Determination of the Apparent Second-Order Rate Constant

An apparent second-order rate constant for the reaction between TC and •OH, denoted as $K_{\bullet \mathrm{OH,TC}}$, was estimated to provide a system-specific kinetic parameter. This estimation was based on the steady-state approximation, using the following equation:

$$K_{\bullet \mathrm{OH,TC}} = K/[\bullet OH]_{\mathrm{steady-state}} \qquad Eq.S8$$

Where:

$K_{\bullet \mathrm{OH,TC}}$ is the observed pseudo-first-order degradation rate constant of TC (s^{-1}) attributed to •OH attack. In this study, the rate constant obtained in the AB-TWPs system (K=1.78×10^{-6} s^{-1}) was used for this calculation, under the assumption that •OH-mediated degradation was the predominant pathway in this system.

$[\bullet OH]_{\mathrm{steady-state}}$ is the steady-state concentration of hydroxyl radicals (mol/L) quantified by EPR spectroscopy, as detailed in Table S3 ($[\bullet OH]_{\mathrm{steady-state}}$ =2.075×10^{-7} mol/L.)

It is crucial to note that this is an apparent value, specific to our heterogeneous experimental system. It reflects the effective reactivity under the influence of competitive quenching processes on the TWPs surfaces and within the solution bulk, and thus cannot be directly compared to the intrinsic rate constant obtained via competition kinetics in homogeneous solutions (Davies, 2016).

Table S1. Two-way ANOVA results for the effects of Group and Time on the measured value.

Source of Variation	Degree of freedom	Sum Sq	Mean Sq	p-value
Group	2	0.148	0.0739	< 0.001
Time	5	0.196	0.0392	< 0.001
Group × Time	10	0.0347	0.00347	< 0.001
Residuals	36	0.00304	0.0000844	< 0.001

Table S2. Post-hoc pairwise comparisons (Tukey's HSD test) among groups.

Comparison	Mean Difference	95% Confidence Interval	p-value
AB-TWPs vs Blank	-0.126	(-0.134, -0.118)	**< 0.001**
B-TWPs vs Blank	-0.092	(-0.100, -0.084)	**< 0.001**
AB-TWPs vs B-TWPs	-0.034	(-0.042, -0.027)	**< 0.001**

Table S3. Pseudo-first-order degradation kinetic parameters of TC in the presence of TWPs under different initial concentrations.

Samples		**Fitted Equation**	***K* (h^{-1})**	***K* ($m^2/mol/s$) ($\times 10^{-4}$)**	**R^2**
High-concentration TC (50 mg/L for TC)	Blank	y=0.0014x + 0.017	0.0014	1.07	0.8341
	B-TWPs (400 mg/L)	y=0.0051x + 0.0174	0.0051	3.88	0.9727
	AB-TWPs (400 mg/L)	y=0.0064x + 0.0223	0.0064	4.87	0.9667
Environmentally relevant TC (100 μg/L for TC)	Blank	y=0.0006x + 0.0845	0.0006	0.457	0.9382
	B-TWPs (10 mg/L)	y=0.0024x + 0.1856	0.0024	1.83	0.9465
	AB-TWPs (10 mg/L)	y=0.0067x + 0.1532	0.0067	5.10	0.9401

Table S4. Comparison of parameters for Langmuir and Freundlich adsorption isotherm models.

Parameter	Symbol	Unit	B-TWPs	AB-TWPs
Langmuir Model				
Max. Adsorption Capacity	Q_m	mg/g	33.40	36.97
Langmuir Constant	K_L	L/mg	0.0480	0.0601
Determination Coefficient	R^2		0.901	0.948
Freundlich Model				
Adsorption Capacity Factor	K_F	mg/g·(L/mg) $^{1/n}$	2.73	5.00
Adsorption Intensity	n		1.94	2.31
Determination Coefficient	R^2		0.838	0.898

Table S5. Atomic percentage of elements on the surface of the sample as determined by XPS.

Atomic %	Samples	
	B-TWPs	AB-TWPs
C-H, C-C	32.24	36.00
C-O	3.58	5.71
C=O	0.47	0.98

Table S6. Concentration of ROS in degradation solution.

Spins	**Samples**	
	B-TWPs	AB-TWPs
·OH (spins/mm^3)	8.97×10^{10}	1.25×10^{11}
$O_2^{\cdot-}$(spins/mm^3)	6.94×10^{11}	5.94×10^{11}
Oxygen center free radical (spins/g)	4.78×10^{17}	5.14×10^{17}

Table S7. Analytical Results of Total Carbon (TC), Inorganic Carbon (IC), and TOC Concentrations in Samples (n=3).

Samples	**TC (mg/L)**	**IC (mg/L)**	**TOC (mg/L)**
Blank	27.80 ± 0.09	0.4162 ± 0.010	27.38 (26.65 - 28.11)
TC+ AB-TWPs (6 hours)	25.93 ± 0.04	0.6272 ± 0.013	25.92 (25.18 - 26.66)
TC+ AB-TWPs (48 hours)	24.46 ± 0.06	1.123 ± 0.022	23.33 (22.56 - 24.10)

Note: TC and IC concentrations are presented as "mean ± standard deviation". TOC concentration is presented as "mean (95% confidence interval)", where the mean was calculated from (TC - IC), and the confidence interval was calculated based on TOC values.

Table S8. Accurate Mass Identification of Degradation Products.

Accurate mass	Molecular formula	Mass deviation (ppm)	Key MS/MS Fragments (m/z)	Confidence Level
418.1268	$C_{20}H_{22}N_2O_8$	-3.16	400.13, 354.13, 208.06	Level 2b
332.1418	$C_{18}H_{20}O_6$	3.55	223.97, 196.96	Level 2b
228.0469	$C_{22}H_{18}NO_7$	-5.74	181.08, 154.12	Level 2b
116.0469	$C_{10}H_{12}NO_6$	-2.67	128.14, 54.26	Level 2b
464.2001	$C_{22}H_{28}N_2O_9$	4.33	432.10, 387.04, 343.05	Level 2b
425.1989	$C_{21}H_{31}NO_8$	-0.26	410.12, 361.20	Level 2b
268.071	$C_{13}H_{16}O_6$	-7.09	241.08, 232.10	Level 2b
428.1356	$C_{22}H_{24}N_2O_7$	-5.70	410.12, 392.14, 337.07	Level 2b
302.1376	$C_{17}H_{18}O_5$	5.83	201.23	Level 2b
228.0659	$C_{10}H_{12}O_6$	2.59	208.17, 180.17, 95.08	Level 2b
126.0923	$C_8H_{14}O$	-6.11	108.16, 70.03	Level 2b

Table S9. Key Factors Influencing the Degradation Behavior of Tire Wear Particles During Aging.

Factor	Relative Abundance in B-TWPs	Relative Abundance in AB-TWPs	Contribution to Degradation Amount	Contribution to Apparent Reaction Rate Constant
C=O	0.385	0.615	0.111	0.184
C-O	0.324	0.676	0.203	0.338
C-OH	0.270	0.720	0.050	0.090
O-C=O	0.380	0.610	**0.310**	**0.521**
Crystalline	0.423	0.577	0.068	0.112
CV	0.417	0.583	0.075	0.124
Fe	0.602	0.398	0.063	0.104
Cu	0.430	0.570	0.061	0.102
EDC	0.419	0.581	0.072	0.119
Zn	0.545	0.455	0.031	0.051
•OH	0.418	0.582	0.074	0.122
EPFRs	0.482	0.518	0.014	0.023
$O_2^{\bullet-}$	0.539	0.461	0.027	0.045
DOM	0.389	0.631	0.133	0.221

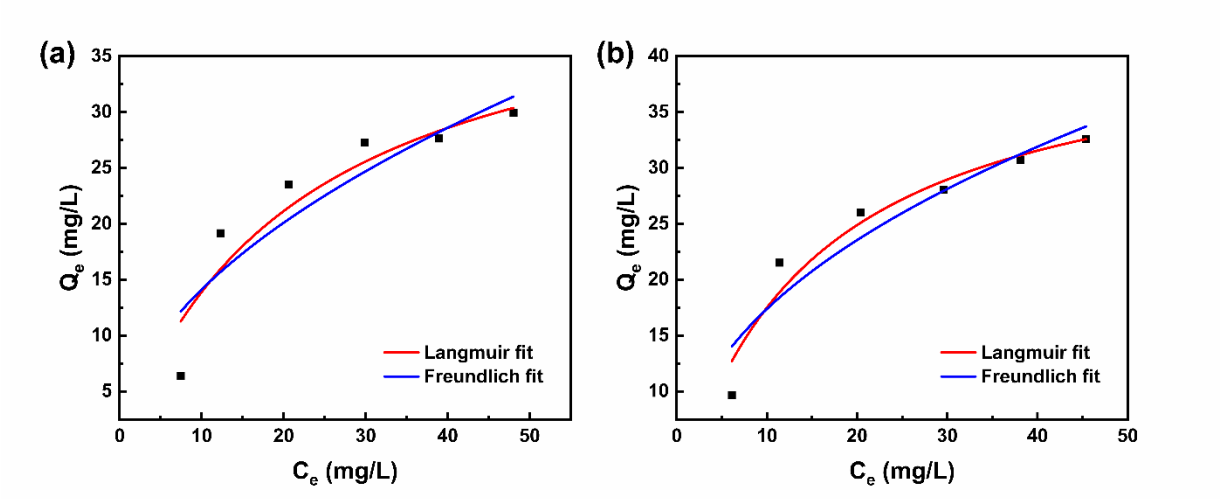

Fig. S2. Adsorption isotherms of TC at elevated concentrations on (a) B-TWPs and (b) AB-TWPs.

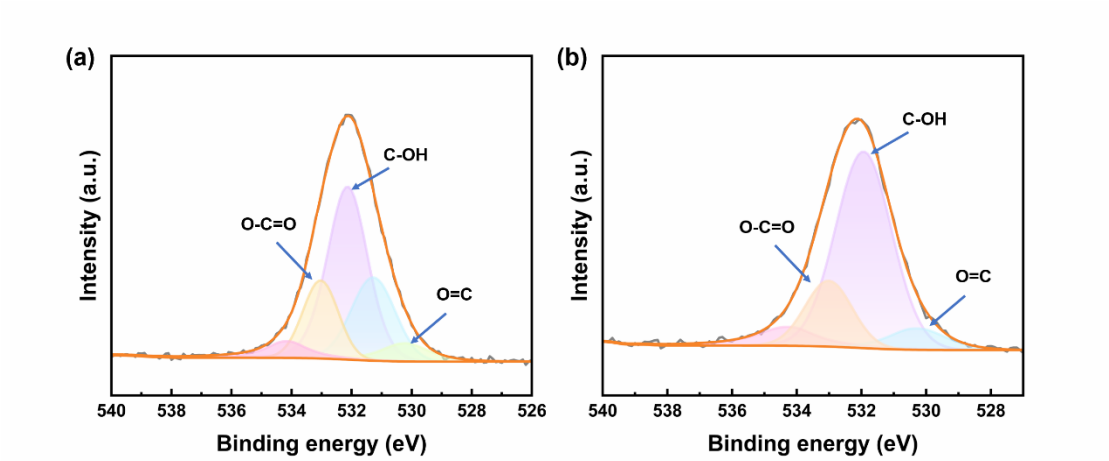

Fig. S3 O_{1s} XPS spectra of (a) B-TWPs and (b) AB-TWPs.

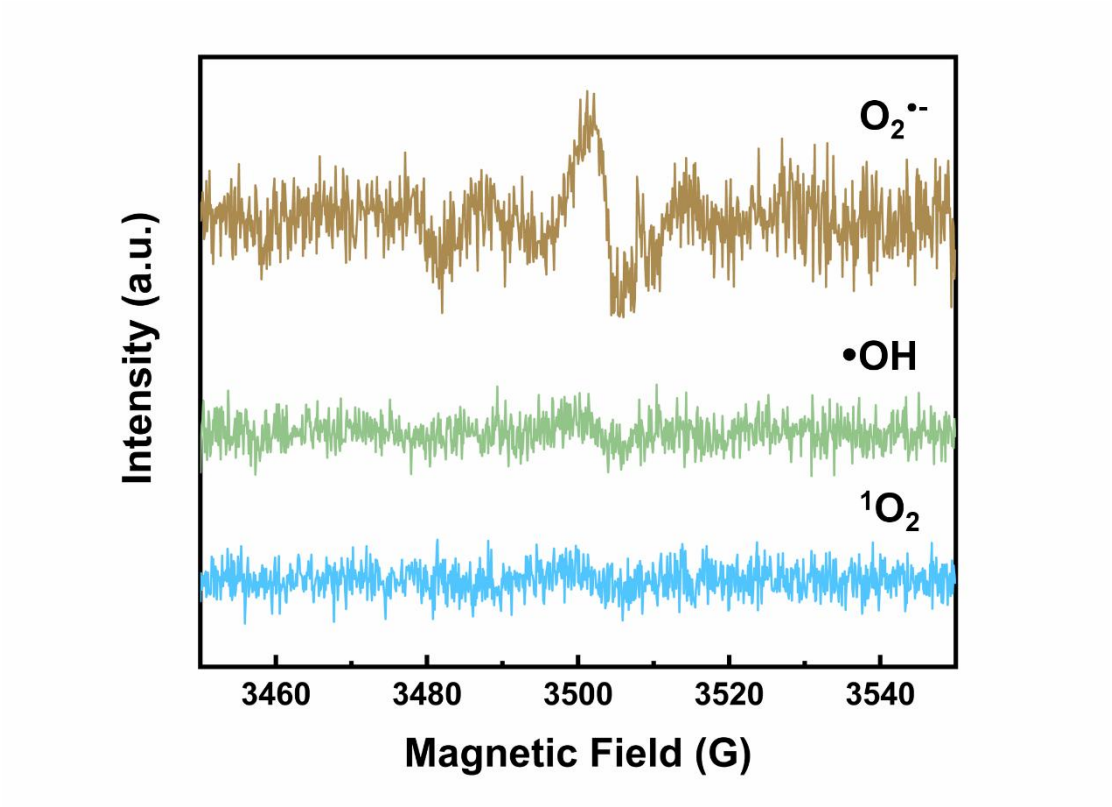

Fig. S4 The EPR spectrum of TC solution.

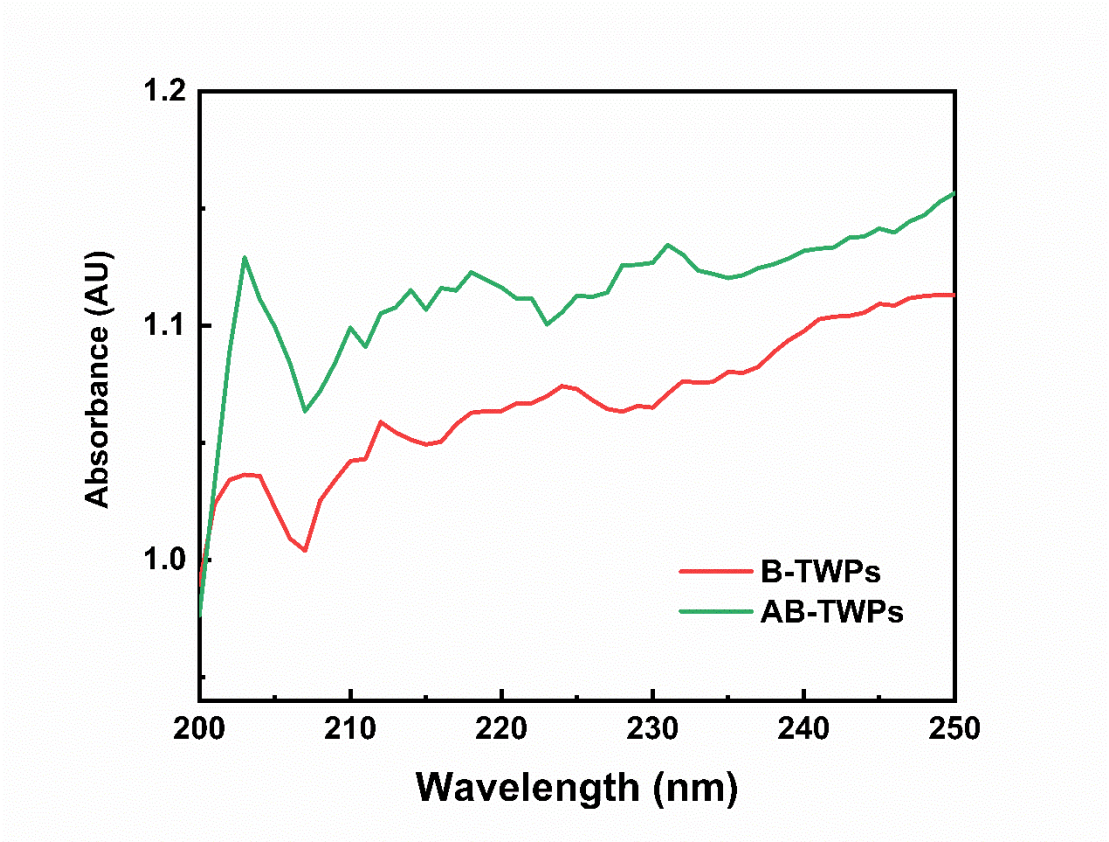

Fig. S5 UV-Vis Absorption Spectra and the Impact of Photo-aging on the Characteristics of Dissolved Organics from TWPs.

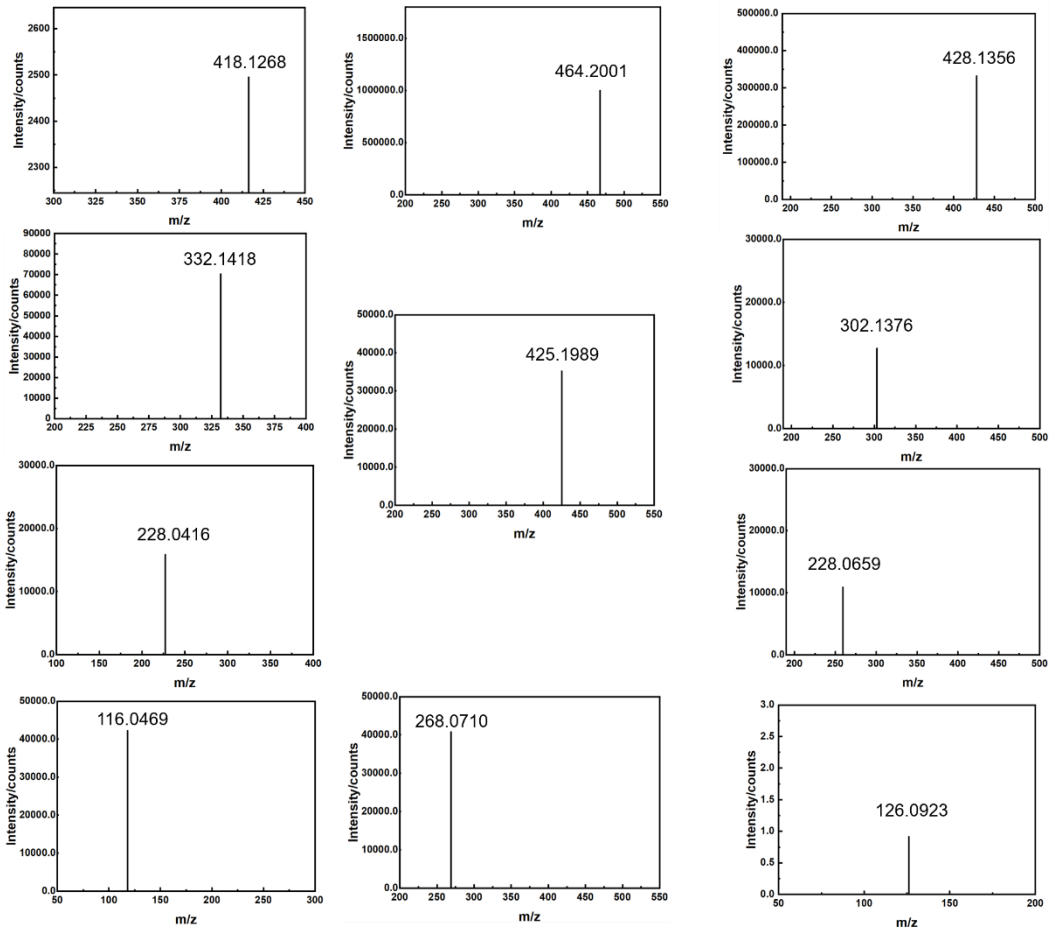

Fig. S6 Mass spectra of TC.

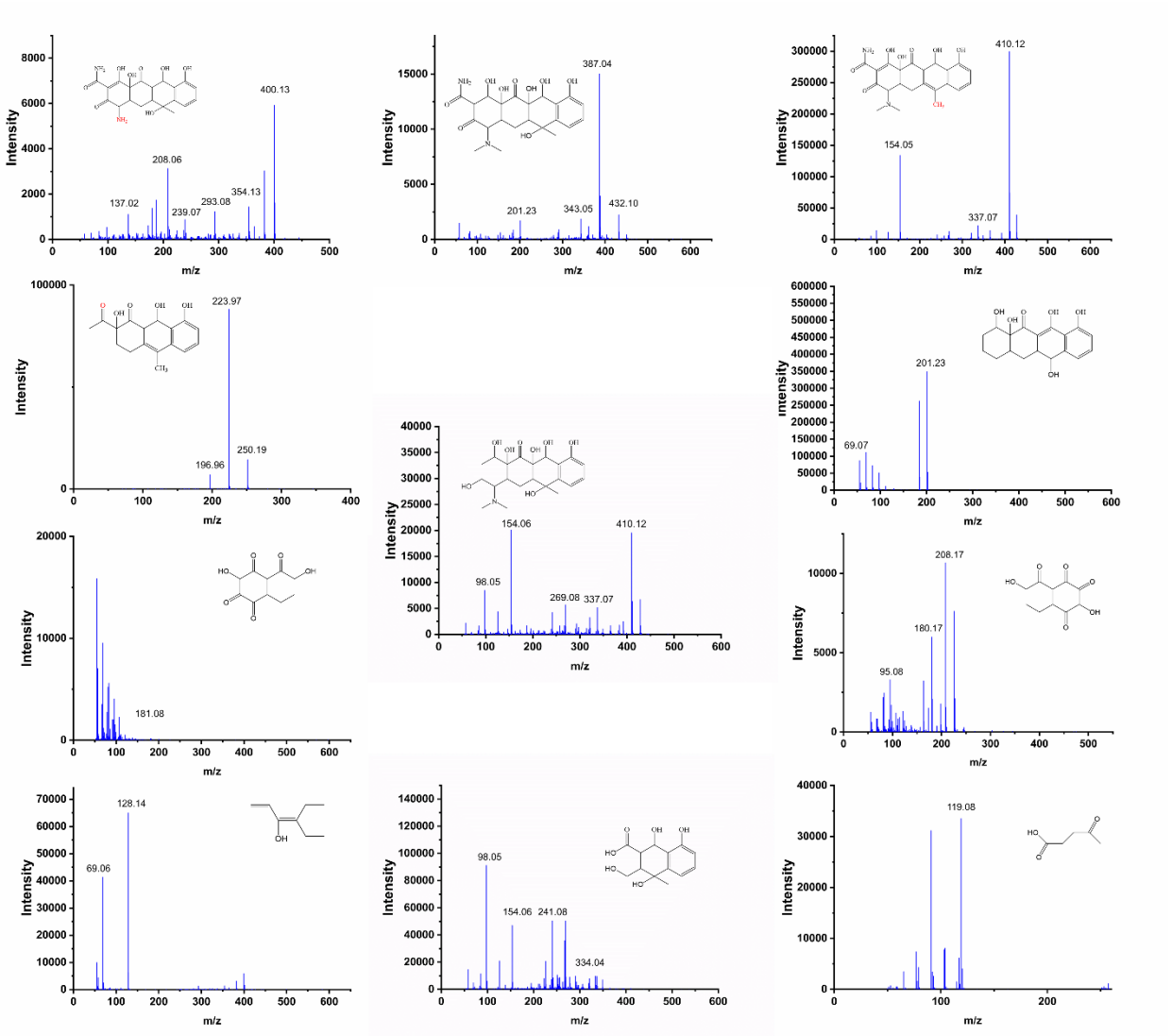

Fig. S7 MS/MS Spectrum of the Degradation Products.

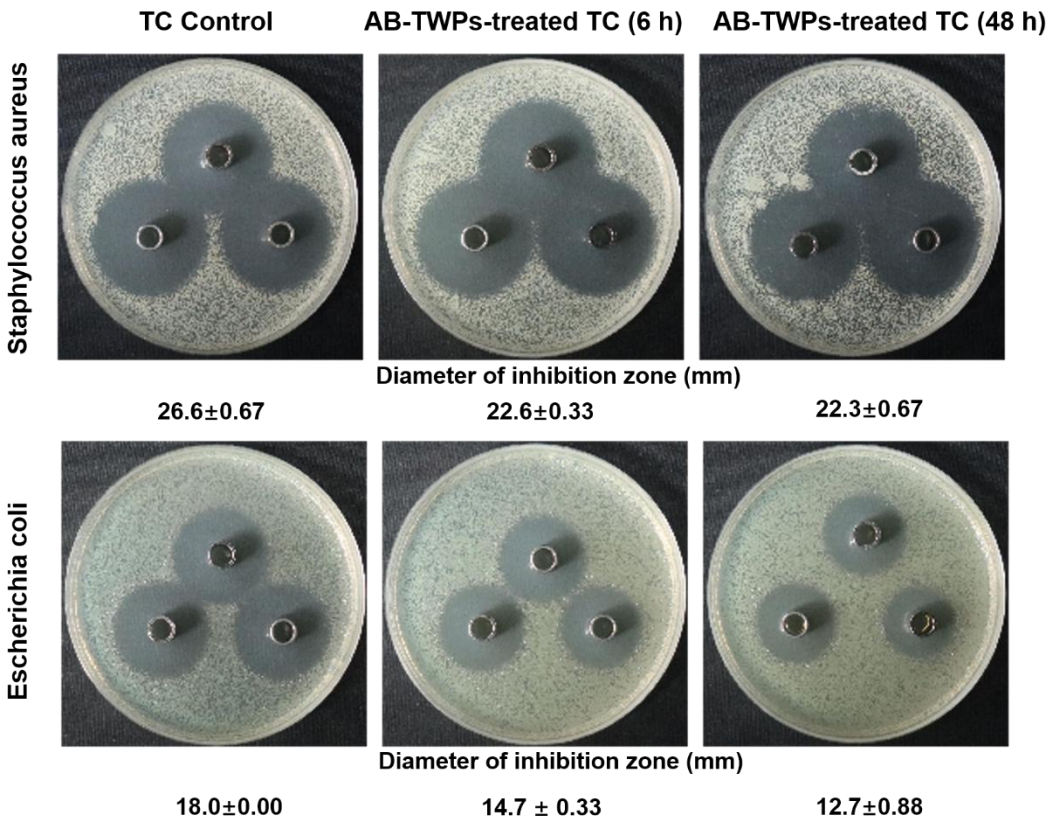

Fig. S8 Inhibitory zones of TC solutions treated with AB-TWPs for different durations against *E. coli* and *S. aureus*.

References

Abd Manan T S B, Khan T, Wan Mohtar W H M, Beddu S, Mohd Kamal N L, Yavari S, Jusoh H, Qazi S, Imam Supaat S K B, Adnan F, Ghanim A A, Yavari S, Machmudah A, Rajabi A, Porhemmat M, Irfan M, Abdullah M T, Abdul Shakur E S B (2020). Dataset on specific UV absorbances (SUVA254) at stretch components of Perak River basin. Data in brief, 30: 105518-105518

Cambier S M, Frankel G S (2014). Coating and Interface Degradation of Coated steel, Part 2: Accelerated Laboratory Tests. ELECTROCHIMICA ACTA, 136: 442-449

Chokejaroenrat C, Watcharatharapong T, T-Thienprasert J, Angkaew A, Poompoung T, Chinwong C, Chirasatienpon T, Sakulthaew C (2024). Decomposition of microplastics using copper oxide/bismuth vanadate-based photocatalysts: Insight mechanisms and environmental impacts. Marine Pollution Bulletin, 201: 116205

Davies M J (2016). Protein oxidation and peroxidation. BIOCHEMICAL JOURNAL, 473: 805-825

Ding L, Yu X, Guo X, Zhang Y, Ouyang Z, Liu P, Zhang C, Wang T, Jia H, Zhu L (2022). The photodegradation processes and mechanisms of polyvinyl chloride and polyethylene terephthalate microplastic in aquatic environments: Important role of clay minerals. Water Research, 208: 117879

Fan X, Zou Y, Geng N, Liu J, Hou J, Li D, Yang C, Li Y (2021). Investigation on the adsorption and desorption behaviors of antibiotics by degradable MPs with or without UV ageing process. Journal of Hazardous Materials, 401

Lei C, Chengkai M, Shanning Y, Xianjuan P, Huanhuan L, Xiangyu C, Haiyang S, Minghong W (2024). Comparison of aging behavior and adsorption processes of biodegradable and conventional microplastics. Chemical Engineering Journal, 502: 157915

Li H, Lin H, Raza S, Zhao Z, Chen S, Wang Y, Zeng Q, Chen C, Yu W, Shen L (2025). Molecular insights in outstanding performance of Ca2+ bridging MXene/ Sodium alginate composite membranes. Water Research, 286

Li K, Hao W, Chen Z, Ye Z (2024). Acute inhibitory effects of tire wear particles on the removal of biological phosphorus：The critical role of aging in improving environmentally persistent free radicals. Environmental Pollution, 360: 124638

Pu Y, Hao Y, Zeng Q, Yang Q, Yang B, Wu Y, Yang X, Sun Y, Wang X, Ma Y, Shi S, Gong Z (2025). Effects of UV-aged tire wear particles (TWPs) on soil microorganisms: Microbial community, microbial metabolism, cell defense and repair, and transmission of ARGs. Journal of Environmental Chemical Engineering, 13(2): 115624

Schymanski E L, Jeon J, Gulde R, Fenner K, Ruff M, Singer H P, Hollender J (2014). Identifying Small Molecules via High Resolution Mass Spectrometry: Communicating Confidence. Environmental Science & Technology, 48(4): 2097-2098

Song Y K, Hong S H, Jang M, Han G M, Jung S W, Shim W J (2017). Combined Effects of UV Exposure Duration and Mechanical Abrasion on Microplastic Fragmentation by Polymer Type. Environmental Science & Technology, 51(8): 4368-4376

Wang J, Wang H, Shen L, Li R, Lin H (2023). A sustainable solution for organic pollutant degradation: Novel polyethersulfone/carbon cloth/FeOCl composite membranes with electric field-assisted persulfate activation. Water Research, 244

Wu M, Zhang M, Shen L, Wang X, Ying D, Lin H, Li R, Xu Y, Hong H (2023). High propensity of

membrane fouling and the underlying mechanisms in a membrane bioreactor during occurrence of sludge bulking. Water Research, 229

Xie M, Yang W, Zhou X, Wang B, Liu J, Xu X, Shen L, Zhang H, Zhang M, Yu W, Teng J, Lin H, Zhao L, Li B (2026). Multiscale thermodynamic insights into membrane fouling control by biochar-activated peroxymonosulfate pretreatment: Synergy of oxidation and adsorption. Water Research, 288

Xie Y, Meng Q, Xu J, Zhang T, Yu C, Pi Y, Guo G, Li Y, Li J, Dong S (2025). New insights into the behavior of coexisting ciprofloxacin photodegradation accelerated by reactive oxygen species generated during aging of polystyrene microplastics. Separation and Purification Technology, 360: 131137

Zhang H, Ma Q, An G, Zhu Y, Sun X, Kawazoe N, Chen G, Yang Y (2025). Development of ag/Ag2O/BiPO4/Bi2WO6/g-C3N4 Z-scheme photocatalyst for high-efficiency tetracycline removal: Characterization, degradation pathway and toxicity assessments. Environmental Functional Materials,

Zhang P, Tang X, Qin N, Shuai Y, Wang J, Wang H, Ouyang Z, Jia H (2024). Advanced understanding of the natural forces accelerating aging and release of black microplastics (tire wear particles) based on mechanism and toxicity analysis. Water Research, 266: 122409